Silicon (2018) 10:921–930
DOI 10.1007/s12633-017-9549-6

ORIGINAL PAPER

Analysis and Optimization of WEDM Performance Characteristics of Inconel 706 for Aerospace Application

Priyaranjan Sharma[1] · D. Chakradhar[1] · Narendranath S.[1]

Received: 12 February 2016 / Accepted: 2 January 2017 / Published online: 3 July 2017

Abstract Wire Electrical Discharge Machining (WEDM) has established itself for manufacturing of precise and complex shape components for aerospace application due to the high quality requirement of aerospace components such as normal residual stress, no cracks, no recast layer, no porosity; still there is a need to optimize the control parameter settings and evaluate the performance characteristics of the WEDM process. The experiments have been conducted on Inconel 706 which is a newly-developed superalloy specially for aircraft application. A hybrid approach has been used to optimize the material removal rate (MRR) as well as surface roughness (SR) and significant control parameters have been identified using analysis of variance (ANOVA). Microstructure analysis revealed the formation of microglobules, melted debris and microholes on the machined surface, but no microcrack was detected due to the high toughness of the alloy. Energy dispersive X-ray spectroscopy (EDAX) has been carried out to study the metallurgical changes in the WED machined surface. The topography analysis of the curved surface revealed the best surface quality of the machined component at low pulse on time and high pulse off time. A thick recast layer of 39.6 μm was observed at high pulse on time and low servo voltage. Microhardness of the machined surface was changed up to a depth of 70 μm due to cyclic thermal loading during the WEDM process.

✉ Priyaranjan Sharma
priya333ranjan@hotmail.com

[1] Department of Mechanical Engineering, National Institute of Technology Karnataka, Surathkal 575025, India

Keywords WEDM · Inconel 706 · Topography · Microstructure · Microhardness · Recast layer

1 Introduction

Nowadays, modern manufacturing industries are continuously looking for complex shaped profiles through difficult-to-cut electrically conductive materials such as superalloy, ceramic and metal matrix composites. Among these materials, nickel-iron-based superalloys are classified as a unique category of materials characterized by the high phase stability of the face centered cubic (FCC) austenitic matrix [1]. Because of their good surface stability, creep resistance at high temperature, corrosion and oxidation resistance, these superalloys are widely used in gas turbines, space vehicles, submarines, rocket engines, nuclear reactors, chemical plants, and structural applications [2]. The conventional machining of nickel-iron-based superalloys (i.e., Inconel 718, Inconel 706) is generally characterized by low surface quality, low productivity and low process stability because of their highly abrasive nature, affinity to react with the tool materials and low thermal diffusivity [3]. The conventional machining processes offer poor surface finish, low dimensional accuracy, high tool wear rate, poor machinability, burr formation and formation of ribbon and snarled chips on the machined components. To overcome these difficulties, non-conventional machining processes are successfully employed.

Among these processes, the Wire Electrical Discharge Machining (WEDM) process exhibits good capability to machine these superalloys components with improved surface quality and dimensional accuracy. With the use of the

WEDM process, it became possible to produce the parts with complex shapes and high precision for the components required in challenging environments such as aircraft turbines, industrial gas turbines, space vehicles, and nuclear reactors. Still, there are some issues in WEDM regarding the surface quality of the machined components. In previous years, a significant research has been carried out to study the surface and subsurface characteristics of the WED machined components. Klocke et al. [4] have made an attempt to enhance the WEDM capabilities for the production of fir tree slots in Inconel 718 superalloy. The standards specified by the turbine industries (Ra<0.8 and t = $\pm 5\mu$ m) were met. The best accuracies and surface integrities were achieved with the standard brass wire. Manufacturing time was reduced to 33% with the usage of high speed cutting wire.

Li et al. [5] have studied the surface roughness (SR) of Inconel 718 during the WEDM using statistical distribution which can provide the spectrum of SR over a wide range of machining conditions. They observed that the average SR value of the rough surface was reduced significantly by a trim cut strategy. Aspinwall et al. [6] have used the minimum damage generator technology (MDGT) in the WEDM process to investigate the SR, microstructure, microhardness and recast layer of Inconel 718. Similarly, Antar et al. [7] have used the MDGT in the WEDM process to evaluate the fatigue response of Udimet 720 superalloy. They found that MDGT with appropriate trim pass strategies enhanced the fatigue performance of the machined components significantly. Li et al. [8] have analyzed the SR, surface topography and white layer formation during WEDM of Inconel 718. They found that SR is equivalent in parallel and perpendicular wire directions. Antar et al. [9] have studied the productivity and surface integrity of Udimet 720 alloy using a coated wire electrode in the WEDM process. They found an increase in productivity up to 70% using the coated wire. In addition, the WEDM process parameters have great influence on the white layer formation of Inconel 718 [10]. The average recast layer thickness varied from 5.10 to 8.51 μm during all machining conditions. Sharma et al. [11] have manufactured complex profile slots through Inconel 706 using the WEDM process for a turbine disk application. It was determined that pulse on time and servo voltage are major contributing factors influencing the productivity and surface integrity of the machined component.

Other than the surface integrity evolution of nickel-based superalloy, some researchers have optimized the WEDM control parameter settings. The mathematical model has been developed by Hewidy et al. [12] to correlate the inter-relationships between WEDM control parameters (i.e., peak current, duty factor, wire tension, water pressure) and performance characteristics (i.e., MRR, wear ratio, SR). Response surface methodology (RSM) is found to be advantageous for identifying the effect of process parameters on output responses. Ramakrishnan and Karunamoorthy [13] have developed the ANN model to predict the performance characteristics of the WEDM process more accurately. The effect of various control parameters such as pulse on time, wire feed, delay time and ignition current were studied while machining of Inconel 718 using the WEDM process. It was observed that the multi-response signal to noise (MRSN) ratio with Taguchi's design is a simple, efficient and more consistent tool for optimizing the multiple quality characteristics. Jangra et al. [14] have combined the grey relational analysis (GRA) with the Taguchi method to optimize MRR and SR simultaneously. Through GRA, grey relational grade (GRG) was used as a performance index to determine the optimum combinition of control parameters for multiple quality characteristics. In the same way, Das et al. [15] have combined the principal component analysis with the Taguchi method for multi-objective optimization. Different techniques to tackle optimization problems in the WEDM process of nickel-based superalloy include the Taguchi method, GRA, weighted principal component analysis (PCA), simulated annealing, desirability approach, etc.

Based on the above studies, a hybrid optimization technique has been developed which combines the Taguchi method with the GRA and PCA. This approach uses the optimum weighted factors to calculate the multiple performance characteristic index more accurately. Literature shows that only a limited number of nickel-iron-based superalloys have been studied using the WEDM process. These superalloys are Inconel 601, Inconel 718, Inconel 825, and Udimet 720. Thus, there is a broad scope to analyze the performance characteristics and optimize the control parameters during the WED machining of a newly-developed superalloy such as Inconel 706. Therefore, an attempt has been made to investigate the optimum set of control parameters of the WEDM process for higher productivity as well as better surface quality of the machined component. Further, microstructure, recast layer thickness, microhardness, surface topography and EDX analysis have been carried out to study the surface and subsurface quality of the machined components.

2 Methodology and Methods

The experiments were conducted on Inconel 706 superalloy which is widely used in turbine disks, diffuser cases, compressor disks, engine mounts, and fasteners. The chemical composition of Inconel 706 is shown in Table 1. This material exhibits a significant increase in stress rupture and tensile yield strength compared to other superalloys. Some

Table 1 Chemical composition of Inconel 706 [16]

Alloy (%)		Ni+ Co	Cr	Fe	Nb+ Ta	Ti	Co	C	Mn	Si	S	Cu	Al	P
Inconel	Min.	39	14.5	Bal	2.5	1.5								
706 alloy	Max.	44	17.5		3.3	2	1	0.06	0.35	0.35	0.02	0.3	0.4	0.02

physical and mechanical properties of Inconel 706 are listed in Table 2.

An 'Electronica Ecocut' WED machine was used to perform the experiments. The WEDM setup is shown in Fig. 1. Moreover, a schematic diagram of the WEDM process is shown in Fig. 2 which illustrates the principle of the WEDM mechanism. Generally, WEDM is categorized as a control electro-thermal machining process in which material is removed from the workpiece by a series of rapid, repetitive and controlled electrical discharges between a wire electrode and the workpiece material. WEDM can cut a complex shape profile through any conductive material with the help of CNC programing and multi-axis movement. For the current study, zinc-coated brass wire was selected as the tool electrode as it has an additional zinc coating on the plain brass wire. This coated wire offers substantial increase in cutting speed over the plain brass wire and is used in situations where a plain brass wire produces an undesirable coating on the machined component. Deionized water was used as a dielectric fluid. Based on the machine performance stability, some parameters are kept constant during the experiment as shown in Table 3.

The control parameters, which are shown in Table 4, were selected based on the preliminary research [11] carried out by the authors. However, the levels of control parameters were defined based on the performance stability of the 'Electronica Ecocut' WED machine. Within the range of these control parameters, no gap shortage and wire breakage problems were recorded.

The initial experimental design was based on a L_9 Taguchi orthogonal array (OA) as shown in Table 5. OA helps to minimize the number of experiments. Each experiment was repeated three times to reduce the variability within the experimental work. The complex profile of Inconel 706 superalloy machined by the WEDM process is shown in Fig. 3.

Table 2 Physical and mechanical properties of Inconel 706 [16]

Properties of Inconel 706	Specification
Density	8.05 g/cm^3
Melting Point	1360 °C
Thermal Conductivity	12.5 W/mK
Modulus of Elasticity	210 kN/mm^2

2.1 Measurement of Performance Characteristics

The material removal rate (MRR) was calculated using Eq. 1. A digital weighing balance having an accuracy of 0.001 g was used to measure the weight of the specimen before and after machining. A surface roughness tester (MITUTOYO Surftest SJ-301) was used to calculate the SR of the specimens with an accuracy of 0.01 μm. The topography of the WED machined surface was recorded using a 3D laser microscope.

$$\text{MRR} = \frac{(w \quad - w_i)}{\rho \times} \tag{1}$$

Where, w is the weight of the specimen after machining; w_i is the weight of the specimen before machining; ρ is the density of the specimen; and is the machining time.

A 'JSM-638OLA' analytical scanning electron microscope was used to study the microstructure and recast layer of the machined component. The microstructure specimens were polished using a sequence of SiC papers followed by diamond paste. The samples were etched with Marble's

Fig. 1 Experimental Setup

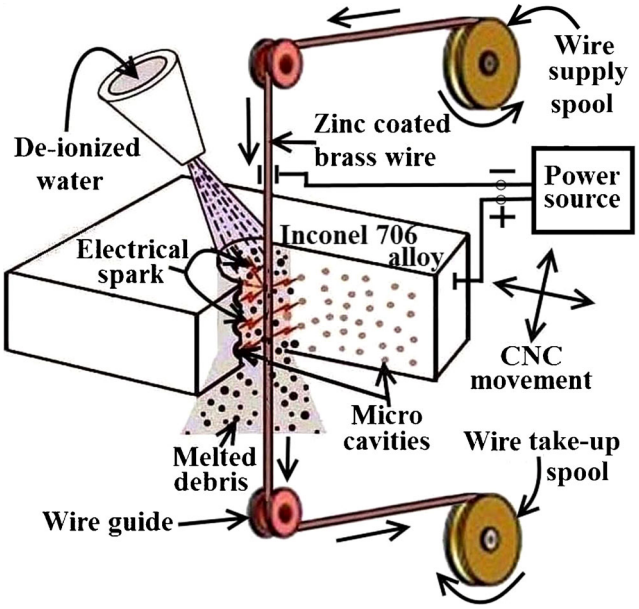

Fig. 2 Schematic illustration of WEDM process

reagent to reveal the grain structure. The etching time was maintained between 110 to 120 sec. An 'OMNI TECH' microhardness tester was used to measure the subsurface microhardness. The microhardness of the subsurface was measured by polishing the cross-section of the machined component. A 'LEST OLS4100' 3D laser microscope was used to capture the surface topography of the machined components. A 'PAN Analytical' XRD machine was used to study the crystal size and crystal structure of WED machined components.

3 Result and Discussion

3.1 Microstructure Analysis of As-received Inconel 706

The microstructure of the as-received Inconel 706 is shown in Fig. 4a which indicates the stable equi-axed grains because of its high phase stability. The grain size analysis was carried out using BIOVIS software as per the ASTM standard E112 which shows the average grain size of 13.5 μm. The chemical composition of Inoconel 706 was confirmed by EDX analysis as shown in Fig. 4b.

Table 3 Constant process parameters used during the WEDM process

Wire Diameter	250 μm
Polarity	Positive
Peak Current	12 A
Peak Voltage	11 V
Servo Feed	2100 mu
Flushing Pressure	2.8 kg/cm^2

Table 4 Control parameters and their levels

Control Parameters	Level-1	Level-2	Level-3
Pulse Duration (µs)	105	115	125
Pulse off Time (µs)	27	45	63
Wire Feed (m/min)	2	4	6
Servo Voltage (V)	24	32	40

3.2 Evaluation of Multi-performance Characteristics

The Taguchi method alone can solve only single objective optimization problems. Therefore, a Taguchi-based hybrid approach was proposed which combines the advantage of GRA as well as PCA. In GRA, data preprocessing is carried out to reduce the range among the performance characteristics. Data pre-processing is the sequence of transferring the original sequence to a comparable sequence. In the comparability sequence all performance values were scaled to [0, 1]. The experimental data corresponding to performance characteristics were normalized using Eqs. 4 and 5.

For larger-the-better performance characteristics,

$$\text{Comparable sequence, } yij = \frac{xij - \min xij}{\max xij - \min xij} \tag{2}$$

For smaller-the-better performance characteristics,

$$\text{Comparable sequence, } yij = \frac{\max xij - xij}{\max xij - \min xij} \tag{3}$$

Where, min xij and max xij are the minimum and maximum value of comparable sequence for jth performance characteristics in ith experimental run.

$$\Delta ij = |y_0 - yij| \tag{4}$$

Where, Δij is the deviation sequence which is defined as the difference of the reference sequence (y) and the com-

Table 5 L_9 Orthogonal Array

Run Order	Pulse on Time (T_{ON})	Pulse off Time (T_{Off})	Servo Voltage (SV)	Wire Feed (WF)
1	105	27	24	2
2	105	45	32	4
3	105	63	40	6
4	115	27	32	6
5	115	45	40	2
6	115	63	24	4
7	125	27	40	4
8	125	45	24	6
9	125	63	32	2

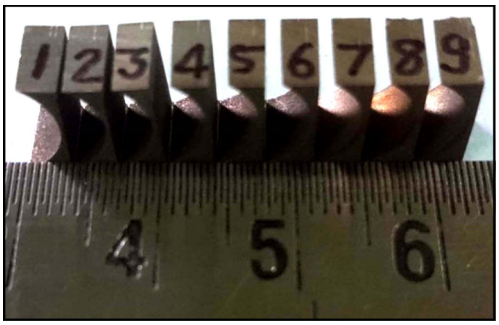

Fig. 3 Curved profile of Inconel 706 machined by the WEDM process

parable sequence (y_{ij}) as shown in Eq. 4. The reference sequence is defined as 1. After data pre-processing, the grey relational coefficient was calculated which expresses the relationship between ideal and actual normalized experimental results. The grey relational coefficient (GRC) was calculated by Eq. 5.

$$\xi ij = \frac{\Delta ij \min + \zeta \Delta ij \max}{\Delta ij + \zeta \Delta ij \max} \tag{5}$$

Where Δ min and Δ max are the minimum and maximum value of the grey relational coefficient for the jth performance characteristics in the ith experimental run. In Eq. 5, ζ is defined as the distinguishing coefficient. The purpose of ζ is to expand or compress the range of the GRC. In the analysis, $\zeta = 0.5$ is considered because this value usually offers moderate distinguishing effects and good stability.

3.2.1 Evaluation of Objective Weight

Principal Components Analysis (PCA) was used to determine the optimum weight of the individual performance characteristics. The multiple performance characteristics array is shown in Eq. 6.

$$X = \begin{bmatrix} x_{11} & \cdots & x_{1n} \\ \vdots & \ddots & \vdots \\ x_{m1} & \cdots & x_{mn} \end{bmatrix}, \; x_{ij}, \; i = 1, 2....m; \; j = 1, 2....n \tag{6}$$

Where, n is the number of performance characteristics and m is the number of the experimental run. The correlation coefficient array is evaluated by Eq. 7.

$$R_{ij} = \left(\frac{Cov(x_{ij}, x_{il})}{\sigma x_{ij} \times \sigma x_{il}} \right), \; j = 1, 2, ...n; \; l = 1, 2, ...n \tag{7}$$

Where, $Cov(x_{ij}, x_{il})$ is the covariance of sequences x_{ij} and x_{il}; σx_{ij} is the standard deviation of sequence x_{ij}; σx_{il} is the standard deviation of sequence x_{il}.

The eigen values and eigen vectors are determined from the correlation coefficient array as shown in Eq. 8.

$$\begin{gathered} \left(R - \lambda_j \mathrm{I}_m\right) V_{ij} = 0 \\ \text{Where, } \sum_{j=1}^{n} \lambda_j = n, \; j = 1, 2, ..., n; \; V_{ij} = [\; _{j1} \;\; _{j2} ... a_{jn}]^T \end{gathered} \tag{8}$$

Where, λ_j is the eigen values and V_{ij} is the eigen vectors corresponding to the eigen values of λ_k. The principal component corresponding to each performance characteristics was calculated using Eq. 9.

$$_{mj} = \sum_{i=1}^{n} X_{mi} . V_{ij} \tag{9}$$

Where, $_{m1}$ is the principal component for MRR and $_{m2}$ is the principal component for SR. The modified grey relational grade (GRG) is a weighted sum of the grey relational coefficients. The overall evaluation of multiple performance

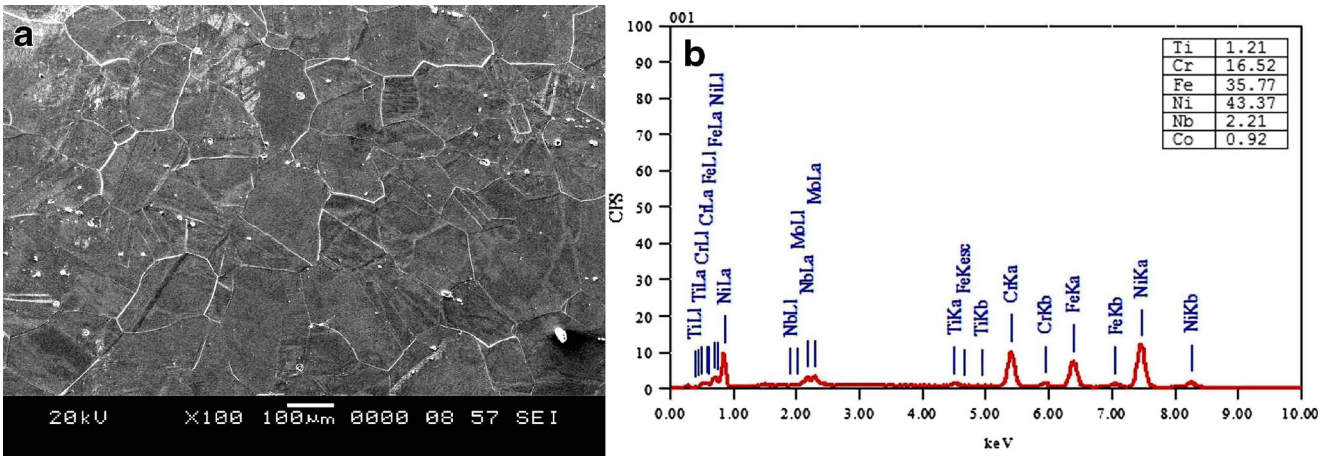

Fig. 4 Microstructure of as-received Inconel 706 (**a**) and EDX analysis of Inconel 706 (**b**)

Table 6 Performance parameters with their grey relational grade (GRG)

SL.	MRR (mm^3 /sec)	SR (mm)	GRC (MRR)	GRC (SR)	Weighted GRC (MRR)	Weighted GRC (SR)	GRG	Rank
1	0.22667	0.00080	0.40269	0.87952	0.20128	0.43963	0.64091	3
2	0.16221	0.00075	0.37211	1.00000	0.1856	0.49985	0.68585	1
3	0.06346	0.00095	0.33333	0.64602	0.16662	0.32291	0.48953	6
4	0.44466	0.00112	0.55767	0.49660	0.27875	0.24822	0.52697	5
5	0.22705	0.00117	0.40288	0.46497	0.20138	0.23241	0.43379	8
6	0.26833	0.00131	0.42527	0.39459	0.21257	0.19724	0.40981	9
7	0.69520	0.00148	1.00000	0.33333	0.49985	0.16662	0.66647	2
8	0.61414	0.00130	0.79579	0.39891	0.39778	0.19930	0.59717	4
9	0.43895	0.00138	0.55211	0.36683	0.27597	0.18336	0.45933	7

characteristics is based on the GRG that was calculated by Eq. 10.

$$\gamma i = \frac{1}{n}\sum_{j=1}^{n} {}^{2}_{mj}\xi ij \tag{10}$$

Where, n is the number of performance characteristics. The GRG indicates the degree of influence that the comparability sequence exerts over the reference sequence. Larger the GRG means that product quality is closer to the ideal value. The GRG with its rank is shown in Table 6. GRG was treated as the larger-the-better multi-performance characteristics. The optimum level of control parameters for high multi-response or high GRG were found to be pulse on time of 105 μs, pulse off time of 27 μs, servo voltage of 32 V and wire feed of 4 m/min as shown in Fig. 5.

3.2.2 Analysis of Variance

Different control factors affect the quality to a different degree. The relative effect of the different factors can be obtained by the decomposition of variance, which is known as ANOVA. The purpose of ANOVA is to investigate which control parameter significantly affects the performance characteristics. This is accomplished by separating the total variability of the grey relational grade. From the ANOVA result of GRG, it was revealed that the pulse on time and pulse off time are the most significant factors affecting the WEDM performance as shown in Table 7.

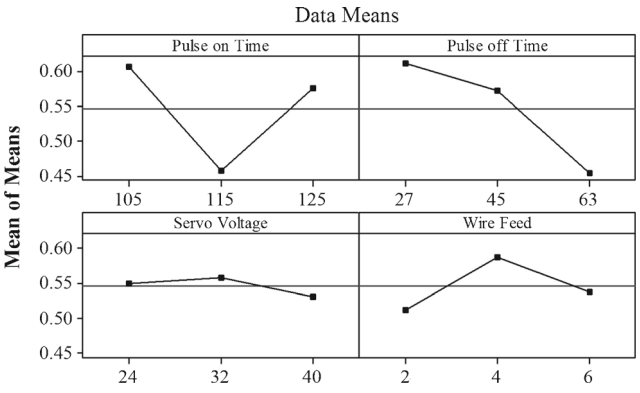

Fig. 5 Main effects plot for means of Grey Relational Grade (GRG)

3.2.3 Confirmation Experiment

Once the optimum WEDM control parameter set was obtained, then confirmation tests were conducted to validate the improvement in multi-performance characteristics index or GRG. The optimal value was predicted using Eq. 11.

$$\eta_{\text{est}} = \eta_{\text{m}} + \sum_{j=1}^{n}(\eta_{\text{j}} - \eta_{\text{m}}) \tag{11}$$

Where, η_{j} is the mean of GRG at optimum level and η_{m} is the overall mean of GRG. The improvement in GRG is shown in Table 8 which indicates the successful completion of the experiment.

3.3 Microstructure Analysis

From the ANOVA results of GRG, it was observed that pulse on time and pulse off time are the most significant

Table 7 ANOVA result of GRG

Control Parameters	Degree of Freedom	Sum of Square	Variance	Percentage of Contribution
T_{ON}	2	0.03684	0.01842	41.91%
T_{Off}	2	0.04093	0.02046	46.56%
SV	2	0.00119	0.0006	1.36%
WF	2	0.00893	0.00447	10.17%
Residual Error		–	–	–
Total	8	0.08790	–	100%

Table 8 Experimental validation of hybrid approach with optimal parameter settings

Response Parameter	Initial process parameters	Optimum response parameters	
		Prediction	Experiment
Level	T_{ON} – 105 μs, T_{Off} – 45 μs, SV – 32 V, WF – 4 m/min	T_{ON} – 105 μs, T_{Off} – 27 μs, SV – 32 V, WF – 4 m/min	T_{ON} – 105 μs, T_{Off} – 27 μs, SV – 32 V, WF – 4 m/min
MRR (mm^3/s)	0.16221	–	0.29452
SR (mm)	0.00075	–	0.00079
GRG	0.68585	0.725029	0.670827

parameters influencing the multiple performance characteristics. The effect of these parameters on microsturcture was investigated to study the surface quality of the machined components. Figure 6a and b are the scanning electron microscope (SEM) images of the WED machined surface at run order 2 and run order 7 respectively. They illustrate the formation of microvoids, microglobules and melted debris on the machined component. From Fig. 6a and b, it was observed that more microvoids and microglobules are formed on the WED machined surface while increasing the pulse on time. At high pulse on time, discharge energy is more which tends to increase the size of the crater formed on the machined surface and thus leads to the poor surface quality of the machined components. Only a few microholes and melted debris were observed in Fig. 6a because of the low discharge energy which thus offers a smooth surface on the machined components. As can be seen from Fig. 6c and d increased pulse off time tends to reduce the formation of microvoids on the machined surface. An increase in pulse off time tends to reduce the spark intensity and increase the cooling time of the workpiece as well as the wire electrode. This in turn, reduces the formation of microvoids and microglobules and thus improves the surface quality of the machined components.

3.4 Surface Topography Analysis

From the 3D surface topography of the curved machined surface, it was observed that surface roughness is highly influenced by pulse on time as well as pulse off time. From Fig. 7a and b it was observed that the topography of the machined surface is rougher at run order 7 compared to

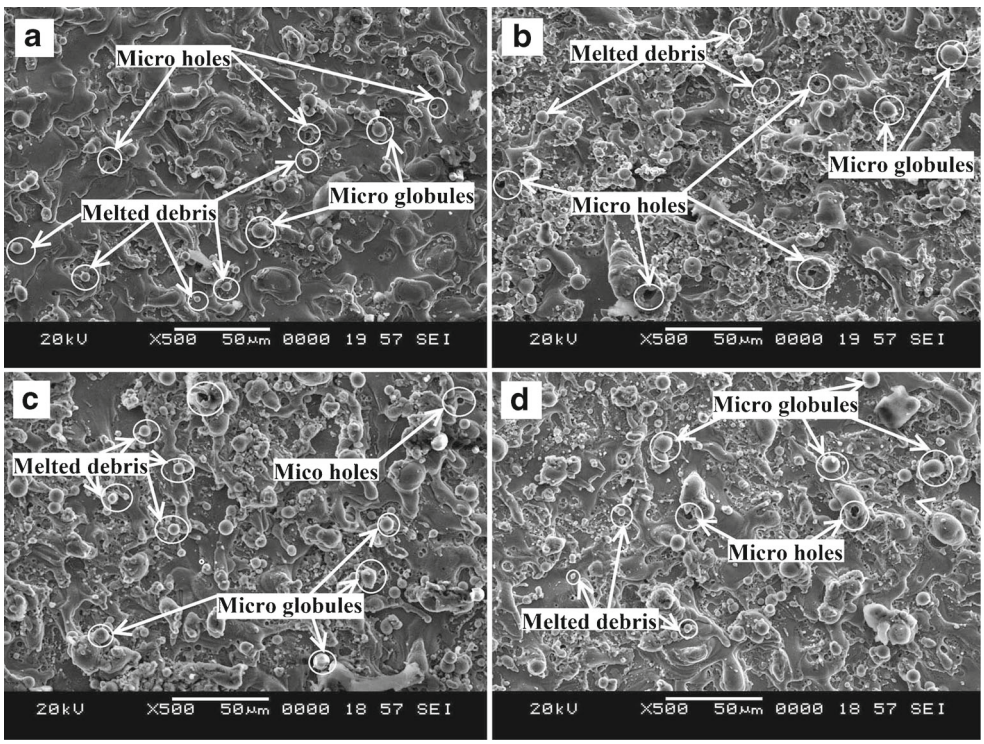

Fig. 6 SEM images of WED machined surface at different run order: **a** run order 2; **b** run order 7; **c** run order 4; **d** run order 6

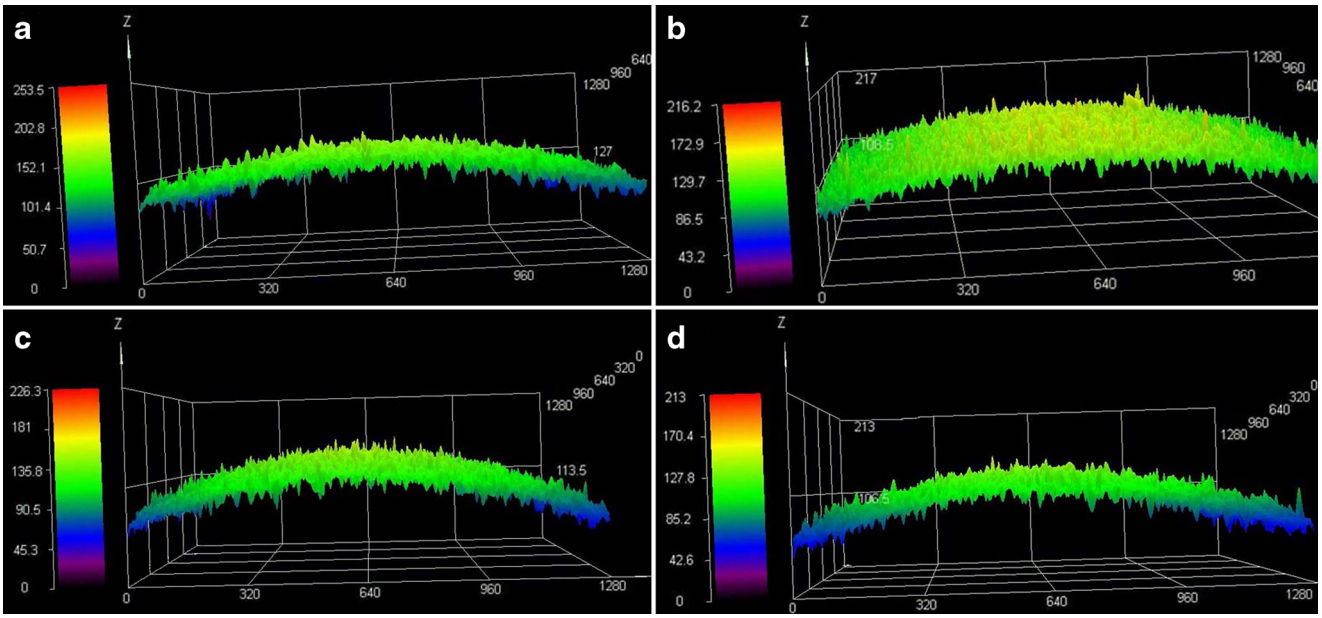

Fig. 7 Machined surface topography at different run order: **a** run order 2; **b** run order 7; **c** run order 4; **d** run order 6

run order 2. This is because an increase of pulse on time leads to an increase in spark intensity and consequently, to an increase in the discharge energy. This, in turn, increases the formation of microvoids and consequently, increases the size of the crater which leads to a poor surface quality of the machined components as observed in Fig. 7b. From Fig. 7c and d, it can be seen that an increase in pulse off time offers a smoother surface on the machined components. High pulse off time tends to reduce the spark intensity and increase the flushing time of melted debris and thus reduces the formation of microvoids on the machined surface leading to better surface quality as shown in Fig. 7d. From the Fig. 7a–d it can be seen that pulse on time has more influence on the surface quality of the machined components compared to pulse off time.

3.5 Microhardness Analysis

Due to the low carbon content of Inconel 706, the WED machined surface becomes softer. This decreases the microhardness up to a certain depth and then maintains the hardness as that of the bulk material. From Fig. 8, it is seen that sub-surface microhardness of the machined component decreases to a depth of 70 μm due to rapid heating and cooling during the WEDM process. The run order 7 shows maximum hardness alterations due to high thermal energy during the WEDM process and thus forms the large size indentation on the machined surface. Moreover, run order 2 shows minimum hardness alterations due to low thermal energy.

3.6 Recast Layer Analysis

The recast layer commonly observed on a WED machined surface is due to melting and resolidification of material, and produces the microstructural changes near the surface layer. As a result of recast layer formation, it creates multiple microvoids and microholes on the machined surface due to significant thermal degradation. From Fig. 9a at run order 7, a thick recast layer was observed due to an increase in discharge energy. At high discharge energy there is a greater propensity of microvoids, microglobules and crater formation resulting in a thick recast layer. Moreover, the microhardness of the recast layer decreases due to metallurgical

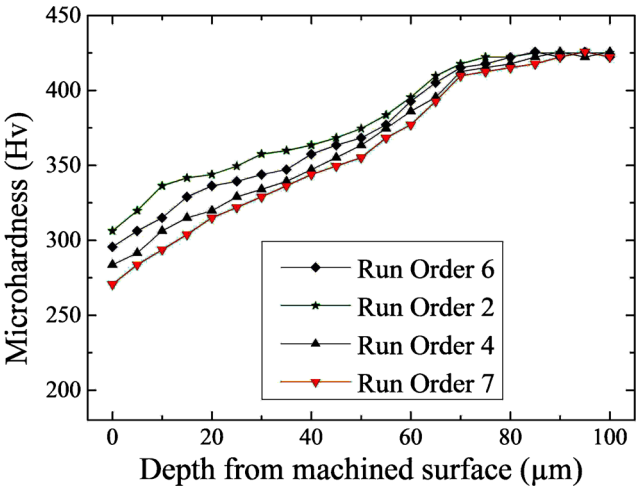

Fig. 8 Subsurface microhardness of WED machined component

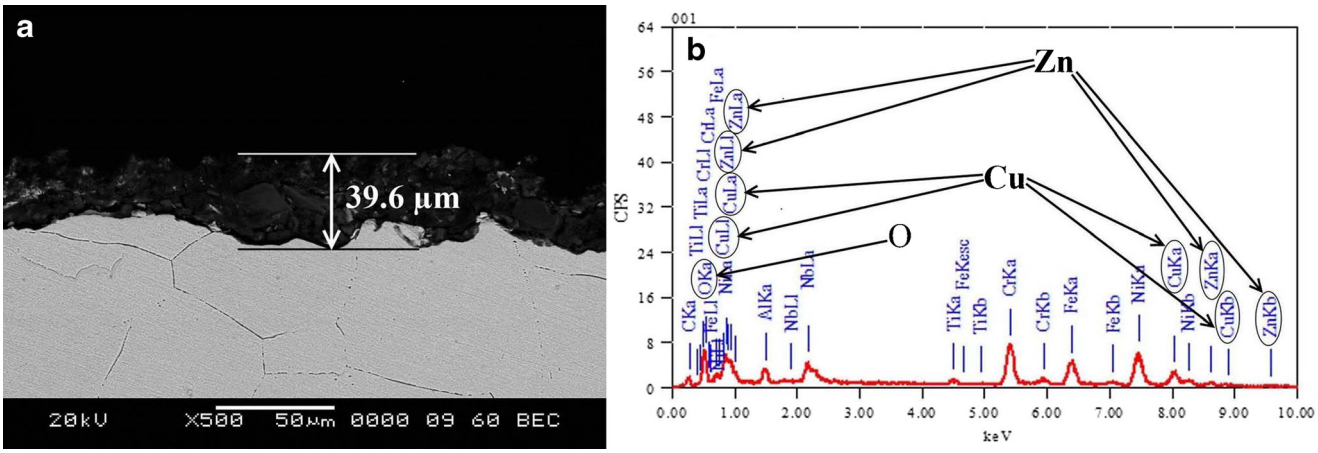

Fig. 9 Microstructure of the cross-section of WED machined surface and EDAX analysis: **a** recast layer formation at run order 7; **b** EDAX of recast surface

changes occurring during the WEDM process. The EDAX analysis of the recast surface revealed the addition of copper and zinc as shown in Fig. 9b. The EDAX analysis also revealed the presence of O (12.96%) in the recast layer and confirms the oxide formation on the machined surface resulting in altered material properties. In addition, tensile residual stresses may be induced within the recast layer due to significant thermal degradation and lead to the lower subsurface hardness of WED machined components. The relation of tensile residual stresses with microhardness already has been reported by Sines and Carlson [17].

3.7 XRD Analysis

The XRD analysis of WED machined surfaces at run order 2 and run order 7 are shown in Fig. 10. The XRD results show that peak intensity is higher at run order 2 compared to run order 7 which exhibits the different crystal structure for both the experimental runs. Generally, high peak intensity corresponds to fine grain structure. Moreover, peak shifting is detected towards the right side which confirms the presence of tensile residual stresses within the WED machined material.

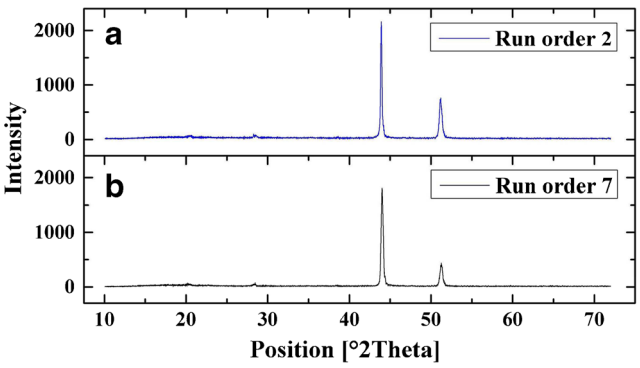

Fig. 10 XRD analysis of WED machined surface at: **a** Run order 2; **b** Run order 7

4 Conclusions

A hybrid optimization technique is reported to improve the multi-performance characteristics of the WEDM process while cutting the complex shape profile through Inconel 706 using zinc-coated brass wire. Further, surface and subsurface characteristics of the WED machined surface have been evaluated. Based on the experimental results, the following conclusions are reported:

- The combined approach of GRA and PCA includes the optimum weightage factor to calculate the GRG more accurately. The highest value of GRG provides the optimum setting of control parameters for maximizing the MRR as well as minimizing the SR.
- The control parameters mainly pulse on time and pulse off time have more influence on multi-performance characteristics index or GRG. The current trends for the MRR and SR are consistent with the findings reported in the literature. Through the usage of the hybrid approach of Taguchi-GRA-PCA, the optimum set of control parameters is found to be pulse on time 105 µs, pulse off time 27 µs, servo voltage 32 V and wire feed 4 m/min.
- The improvement in GRG was found to be 0.0428 which validates the experiment results. The experimental error was 3.27% which is quite considerable. The PCA method combined with GRA proved an easy and effective approach to determine the objective weight of WEDM performance characteristics.
- Microstructure analysis revealed that microvoids, microholes and microglobules are more prominent at

run order 7 due to high discharge energy and thus offer a rough surface on the machined component whereas no microcracks were noticed due to the high toughness of alloy.

- Surface topography analysis of the curved profile revealed that the best surface quality of the machined component was observed at run order 2 due to low spark intensity and thus offering a smooth and fine surface on the machined component. Moreover, surface topography turns out to be rough at run order 7 due to high thermal energy of the spark.
- Microhardness of the WED machined surface decreases to a depth of 70 μm and thereafter it maintains the hardness as that of bulk material. The run order 7 has shows relatively lower hardness of the machined component due to high discharge energy during the WEDM process.
- Recast layer analysis revealed the formation of a thick layer at run order 7 due to increase in spark intensity and thus resulting in formation of more microvoids and microholes on the machined surface. The average recast layer thickness was 39.6 μm at run order 7 although highly variable in nature.
- The microhardness of the recast layer decreased due to metallurgical changes occuring during the WEDM process. The EDX analysis of the recast surface revealed the addition of Cu, O and Zn since only 0.6% Cu is present in Inconel 706 with no zinc and oxygen. Due to cyclic thermal loading during the WEDM process, residual stress may be induced within the recast layer resulting in a lower subsurface hardness.
- XRD analysis of the WED machined surface revealed the changes in crystal structure at different experimental settings. Moreover, peak shifting was detected towards the right side which confirms the presence of tensile residual stresses within the WED machined material.

Acknowledgments This work is partially supported by the Department of Science and Technology (DST), Government of India under the project reference number SB/S3/MMER/0067/2013. The authors would like to thank the DST for its funding support.

References

1. Campbell FC (2006) Manufacturing technology for aerospace structural materials. Elsevier
2. Pollock TM, Tin S (2006) Nickel-based superalloys for advanced turbine engines: chemistry, microstructure and properties. J Propuls Power 22(2):361–374
3. Choudhury IA, El-Baradie MA (1998) Machinability of nickel-base super alloys: a general review. J Mater Process Technol 77(1):278–284
4. Klocke F, Welling D, Klink A, Veselovac D, Nöthe T, Perez R (2014) Evaluation of advanced wire-EDM capabilities for the manufacture of fir tree slots in Inconel 718. Procedia CIRP 14:430–435
5. Li L, Wei XT, Li ZY (2014) Surface integrity evolution and machining efficiency analysis of W-EDM of nickel-based alloy. Appl Surf Sci 313:138–143
6. Aspinwall DK, Soo SL, Berrisford AE, Walder G (2008) Workpiece surface roughness and integrity after WEDM of Ti–6Al–4V and Inconel 718 using minimum damage generator technology. CIRP Ann Manuf Technol 57(1):187–190
7. Antar MT, Soo SL, Aspinwall DK, Sage C, Cuttell M, Perez R, Winn AJ (2012) Fatigue response of Udimet 720 following minimum damage wire electrical discharge machining. Mater Des 42:295–300
8. Li L, Guo YB, Wei XT, Li W (2013) Surface integrity characteristics in wire-EDM of Inconel 718 at different discharge energy. Procedia CIRP 6:220–225
9. Antar MT, Soo SL, Aspinwall DK, Jones D, Perez R (2011) Productivity and workpiece surface integrity when WEDM aerospace alloys using coated wires. Procedia Engineering 19:3–8
10. Newton TR, Melkote SN, Watkins TR, Trejo RM, Reister L (2009) Investigation of the effect of process parameters on the formation and characteristics of recast layer in wire-EDM of Inconel 718. Mater Sci Eng A 513:208–215
11. Sharma P, Chakradhar D, Narendranath S (2015) Evaluation of WEDM performance characteristics of Inconel 706 for turbine disk application. Mater Des 88:558–566. doi:10.1016/j.matdes.2015.09.036
12. Hewidy MS, El-Taweel TA, El-Safty MF (2005) Modelling the machining parameters of wire electrical discharge machining of Inconel 601 using RSM. J Mater Process Technol 169(2):328–336
13. Ramakrishnan R, Karunamoorthy L (2008) Modeling and multi-response optimization of Inconel 718 on machining of CNC WEDM process. J Mater Process Technol 207(1):343–349
14. Jangra K, Grover S, Aggarwal A (2011) Simultaneous optimization of material removal rate and surface roughness for WEDM of WC-Co composite using grey relational analysis along with Taguchi method. Int J Ind Eng Comput 2(3):479–490
15. Das MK, Kumar K, Barman TK, Sahoo P (2013) Optimization of surface roughness and MRR in EDM using WPCA. Procedia Eng 64:446–455
16. Technical bulletin: Inconel alloy 706 (Publication number SMC-091), Special Metals Corporation. Retrieved from (http://www.specialmetals.com/assets/documents/alloys/inconel/inconel-alloy-706.pdf)
17. Sines G, Carlson R (1952) Hardness measurement for determination of residual stress. Bull Amer Soc Testing Mater 180:35–37